Amplified waveguide teleconnections along the polar front jet favor summer temperature extremes over northern Eurasia

Xu, Peiqiang; Wang, Lin; Vallis, Geoffrey K.; Geen, Ruth; Screen, James A.; Wu, Peili; Ding, Shuoyi; Huang, Ping; Chen, Wen

DOI:
10.1029/2021gl093735

Geophysical Research Letters

RESEARCH LETTER
10.1029/2021GL093735

Key Points:

- Summer temperature extremes over northern Eurasia are linked with amplified waveguide teleconnections embedded in the polar front jet
- The above relationship is robust in both observations and large-ensemble simulations with multiple climate models
- The relation is particularly strong for hot and cold events over eastern Europe and western Russia

Supporting Information:

Supporting Information may be found in the online version of this article.

Correspondence to:

L. Wang,
wanglin@mail.iap.ac.cn

Citation:

Xu, P., Wang, L., Vallis, G. K., Geen, R., Screen, J. A., Wu, P., et al. (2021). Amplified waveguide teleconnections along the polar front jet favor summer temperature extremes over northern Eurasia. *Geophysical Research Letters*, *48*, e2021GL093735. https://doi.org/10.1029/2021GL093735

Received 6 APR 2021
Accepted 7 JUN 2021

Amplified Waveguide Teleconnections Along the Polar Front Jet Favor Summer Temperature Extremes Over Northern Eurasia

Peiqiang Xu[1], Lin Wang[1], Geoffrey K. Vallis[2], Ruth Geen[2], James A. Screen[2], Peili Wu[3], Shuoyi Ding[4], Ping Huang[1], and Wen Chen[1]

[1]Center for Monsoon System Research, Institute of Atmospheric Physics, Chinese Academy of Sciences, Beijing, China, [2]College of Engineering, Mathematics and Physical Sciences, University of Exeter, Exeter, UK, [3]Met Office Hadley Centre, Exeter, UK, [4]Department of Atmospheric and Oceanic Sciences and Institute of Atmospheric Sciences, Fudan University, Shanghai, China

Abstract

An apparent increase in the frequency of summer temperature extremes over northern Eurasia has been observed in the past decade. Some of these high-impact events were associated with amplified waveguide teleconnections embedded in the polar front jet, but it remains unclear if extreme temperatures are robustly and routinely related to amplified waves along the polar front jet. This study systematically examines relationships between planetary wave activity and temperature extremes using observations, reanalysis, and large-ensemble simulations from multiple climate models. Months with extreme temperatures over northern Eurasia generally have amplified wave activity along the polar front jet, whereas months with near-average temperatures tend to have attenuated wave activity. Waveguide teleconnections are particularly amplified during extremely hot and cold summer months over eastern Europe and western Russia. These findings demonstrate the important role of waveguide teleconnections along the polar front jet in generating regional temperature extremes over northern Eurasia.

Plain Language Summary

Atmospheric circulation anomalies move horizontally across Earth. At a particular location, this can be seen in the passage of low- and high-pressure systems over time, much like the peaks and troughs of an ocean wave. Sometimes these atmospheric waves can become trapped, preventing their northward or southward migration, and are guided predominantly west to east along a common path, and when they do this, they often grow in amplitude. Amplified atmospheric waves may be a cause of prolonged heatwaves, such as those that occurred in eastern Europe and western Russia in summer 2010 and that resulted in 55,000 deaths and economic losses of more than $15 billion. This study examines the relationship between wave activity and summer temperature extremes over northern Eurasia. We find that wave activity tended to be greater than normal during those summer months that had extreme temperatures. In contrast, wave activity was commonly less during months with near-average temperatures. In particular, waves were especially amplified during extremely hot and cold summer months over eastern Europe and western Russia. This work helps to understand the causes of extreme heat waves over northern Eurasia in order that society may be better prepared when they occur.

1. Introduction

Waveguide teleconnections along the tropospheric jet streams can profoundly affect surface weather and cause weather extremes in the middle-to-high latitudes (Chowdary et al., 2019; Screen & Simmonds, 2014). The most noted waveguide teleconnection, the circumglobal teleconnection (CGT), propagates along the subtropical jet (Branstator, 2002; Branstator & Teng, 2017; Ding & Wang, 2005). An enhanced CGT pattern has been suggested as a cause of recent weather extremes, such as the Russian heatwave, northern China heatwave, and Pakistan floods that co-occurred in 2010 (Trenberth & Fasullo, 2012). Recent work has speculated that wave-like circulation patterns, such as the CGT, will become amplified in a warming world, potentially leading to more extreme weather (Coumou et al., 2018; Francis & Vavrus, 2012; Liu et al., 2012; Mann et al., 2017; Petoukhov et al., 2013; Tang et al., 2014). However, robust evidence in support of such proposed changes is lacking (Blackport & Screen, 2020a, 2020b; Screen & Simmonds, 2013; Teng et al., 2016; Teng & Branstator, 2019; Wills et al., 2019).

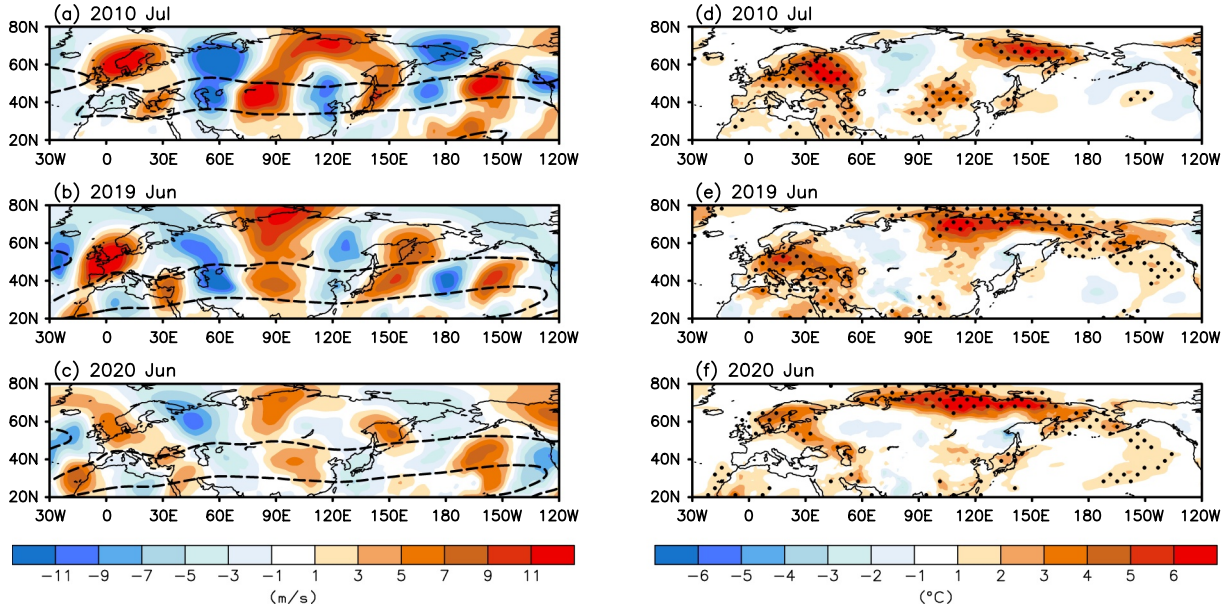

Figure 1. The monthly mean 250-hPa meridional wind (V250, shading) anomalies in (a) July 2010, (b) June 2019, and (c) June 2020, respectively. (d)–(f) are the same as (a)–(c), but for the monthly mean of daily maximum surface temperature (T_{max}, shading). Contours in (a)–(c) indicate the climatological 250-hPa zonal wind speed that exceeds 15 m/s. Stippling in (d)–(f) indicate the TX95p is eight times more than climatology.

Waveguide teleconnections propagating along the polar front jet (PFJ) (Nakamura & Fukamachi, 2004; Schubert et al., 2011; Xu et al., 2019) have received much less attention than those propagating along the subtropical jet. One reason for this may be that the zonal wind speed along the PFJ is weaker than along the subtropical jet, and so the waveguide effect of the PFJ was thought to be weaker than the subtropical jet. However, although the zonal wind speed and lateral wind shear are weaker along the PFJ, the meridional gradient of stratification becomes very strong in boreal summer, making the PFJ an efficient waveguide in summer, comparable to subtropical jet (Iwao & Takahashi, 2008). In addition, Xu et al. (2019) and Xu, Wang, Chen, et al. (2020) found the dominant atmospheric mode inherent in the PFJ is a zonally oriented wave-like pattern along the PFJ, further demonstrating the ability of the PFJ to act as a waveguide in the summer.

Figure 1 presents monthly mean anomalies of the meridional wind at 250-hPa (V250, left panels) and of the daily maximum surface temperature (T_{max}, right panels) during three example months in the last decade, which featured extreme temperature anomalies over Eurasia. In July 2010, a record-breaking heatwave hit eastern Europe and western Russia (Figure 1d), resulting in 55,000 fatalities and economic losses of more than $15 billion (Barriopedro et al., 2011). In June 2019, record-breaking heat waves occurred over central Europe (Figure 1e), leading to temperatures exceeding 45°C, and France, where a red weather alert was issued for the first time in recorded history (Sousa et al., 2020; Xu et al., 2021; Xu, Wang, Liu et al., 2020). In June 2020, an unprecedented heatwave in northern Siberia (Figure 1f) fueled an enormous outbreak of wildfires on tundra underpinned by permafrost. The severity of the heatwaves can be measured by the 95th percentile of daily maximum temperature (TX95p), defined as the percent of days where T_{max} is larger than the calendar day 95th percentile based on a 5-day window for 1958–2018. The regions hit by the three heatwaves all featured extreme value of TX95p that is eight times more than its climatology (Figures 1d–1f). In all cases, pronounced planetary wave activity can be observed along the subtropical jet (Figures 1a–1c). But in addition, a closer examination of the V250 anomalies reveals there was also amplified wave activity along the PFJ over northern Eurasia. The zonal orientation of these planetary waves suggests a waveguide along the PFJ. The close geographical coincidence between the T_{max} and V250 anomalies over northern Eurasia indicates that, in these specific months, teleconnections along the PFJ were a dominant cause of the observed temperature extremes.

Table 1
The Multi-Models LE Datasets Used in This Study

Modeling center	Model version	Model resolution	No. of members	Years	Reference
NCAR	CESM1	1.3° × 0.9°	40	1920–2005	Kay et al. (2015)
GFDL	CM3	2.0° × 2.5°	20	1920–2005	Sun et al. (2018)
CCCma	CanESM2	2.8° × 2.8°	50	1950–2005	Kirchmeier-Young et al. (2017)
CSIRO	MK3.6	1.9° × 1.9°	30	1850–2005	Jeffrey et al. (2013)

Although there appears to be a close relationship between temperature extremes and waveguide teleconnections along the PFJ in these three months, to determine whether or not the relationship is robust requires looking at larger samples. Therefore, a better understanding of the role of waveguide teleconnections along the PFJ in causing such temperature extremes over middle-to-high latitudes is essential, which is the aim of this study.

2. Data and Methods

Monthly mean and four-times daily T_{max} and V250 are from the Japanese 55-year Reanalysis (JRA-55) data set, with 1.25° latitude by 1.25° longitude resolution (Kobayashi et al., 2015). Monthly mean surface temperature (Ts) is from the Climatic Research Unit (CRU) high-resolution gridded data set version 4.04 (CRU TSv4.04) (Harris et al., 2020). The analyzed period for JRA-55 and CRU TSv4.04 is the overlapping period of two datasets, which is 1958–2019. In order to compensate for the limited cases of extreme events in observations, we also use large ensembles (LE) of historical simulations from four Coupled Model Intercomparison Project 5-class (CMIP5-class) Earth System Models (ESMs) (Deser et al., 2020), forced with historical emissions. Analyzed periods and other information about LE datasets are listed in Table 1.

This study focuses on June-July-August (JJA) over Eurasia, when and where the waveguide effect of PFJ is the strongest, and when and where the geographical boundary between the PFJ and subtropical jet is the clearest (Xu, Wang, Chen, et al., 2020). Monthly anomalies are calculated by removing the relevant climatological monthly mean at each grid-point. In order to eliminate the signal from global warming from observations, the global-mean Ts has been subtracted from the grid-point values. For LE simulations, the temporal evolution of the ensemble average of Ts and V250 has been subtracted for each grid-point from the grid-point values in each model.

Following Screen and Simmonds (2014), the absolute values of Ts anomalies (|Ts'|) are used to represent the magnitude of temperature anomalies because teleconnections tend to induce both positive and negative temperature anomalies, depending on the geographical location and the wave phase. For observations, "extreme" and "near-average" months are defined as the 30 cases (approximately 16%) with largest |Ts'| and smallest |Ts'|, respectively, over northern Eurasia (land area over 15°W–180°E, 50°N–80°N) where PFJ waveguide persists (Xu et al., 2019; Xu, Wang, Chen, et al., 2020; Xu, Wang, Liu, et al., 2020), or at each grid point. For LE simulations, the extreme and near-average months are defined as months in which the target area or point falls above the 95% quantile and below the 5% quantile of the probability density distribution (PDF) of |Ts'|, respectively. The 30 cases in observations and 5% or 95% quantiles in LE simulations are chosen somewhat arbitrarily to balance the extremity and the size of the selected samples, and the major conclusions remain similar if slightly different criteria are used. Although extreme events usually occur on sub-monthly timescales, extreme monthly temperature anomalies could indicate the presence of prolonged temperature extreme events (Alexander & Perkins, 2013; Coumou et al., 2013; Coumou & Robinson, 2013), as shown in Figure 1.

In order to measure the activeness of waveguide teleconnections along the PFJ, a wave activity index (WAI) is defined as the area-weighted average of absolute values of V250 anomalies (|V250'|) over northern Eurasia (15°W–180°E, 50°N–80°N). Here, we note that the term *wave activity* we used here is different from the wave activity used in classical wave theory, which indicates the propagation direction of wave packets. The definition of WAI is employed for two reasons. First, the use of meridional wind can put more emphasis on anomalies with shorter zonal scales, and thus is a good variable to extract waveguide teleconnections

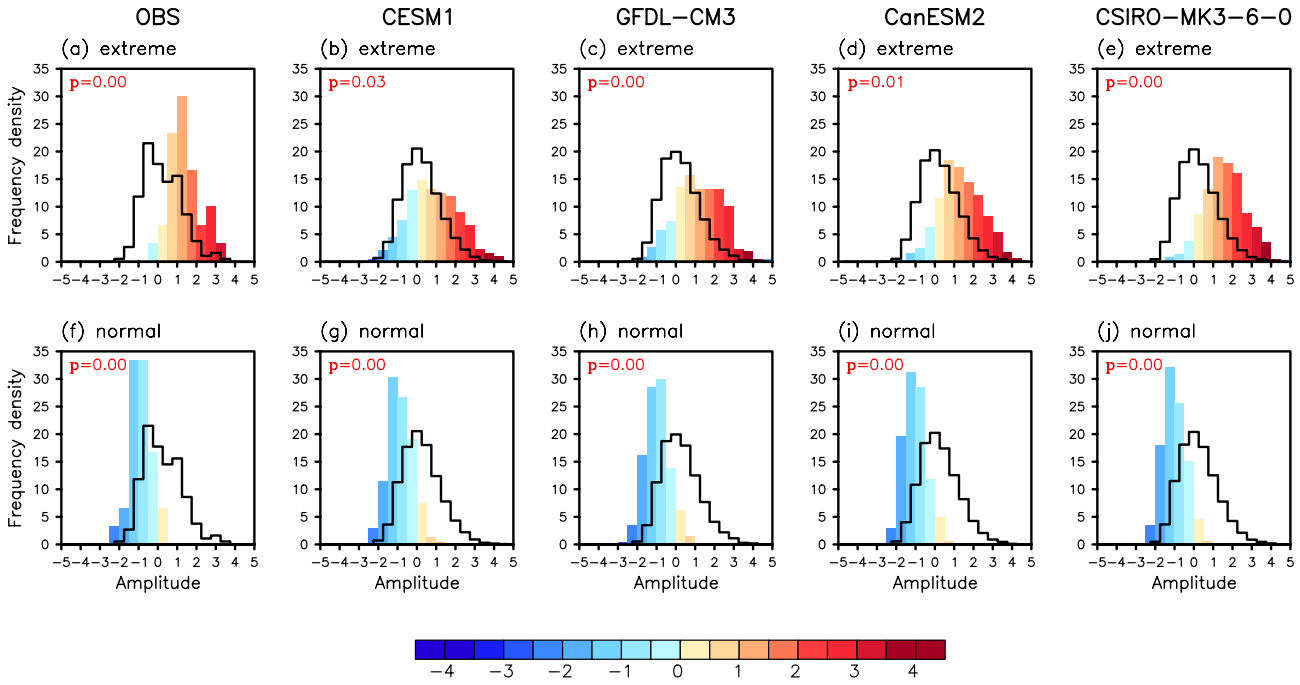

Figure 2. (a) Probability density distributions (PDFs) for normalized wave activity index (WAI) along the polar front jet (PFJ) during summer months of land-based extreme temperature over northern Eurasia (shading) and climatology (all summer months; contour). (f) is the same as (a), but during summer months of near-normal temperature. (b) and (g), (c) and (h), (d) and (i), and (e) and (j) are the same as (a) and (b), but for LE simulations of NCAR-CESM1, GFDL-CM3, CCCma-CanESM2, and CSIRO-MK3.6, respectively. The darkness of shading corresponds to the WAI anomalies in the abscissa and is only used for visual convenience. The *p* values of *t* statistics are labeled in the upper left corner, with red text indicating values that are statistically significant at the 95% confidence level.

compared to geopotential height or streamfunction (Branstator, 2002). Second, the PFJ waveguide, indicated by the maximum value of meridional gradient of potential vorticity (PV) (Figure S1a), is located over northern Eurasia (15°W–180°E, 50°N–80°N). Due to the trapping effect induced by the PFJ waveguide, the Rossby wave activities, indicated by the variance of V250 (Figure S1b), are also strong over northern Eurasia. Therefore, |V250′| can reflect the fluctuations of waveguide teleconnections along the PFJ to a large extent. In the months with large WAI, the zonally oriented wave-like pattern is evident (Figure S2), and the composited V250 variance is enhanced along the PFJ over the northern Eurasia (Figure S4). In the months with small WAI, in contrast, the wave-like pattern is unclear, and the composited V250 variance is weak (Figure S3). These results suggest that the WAI can physically reflect the activeness (amplitude or frequency) of waveguide teleconnections along the PFJ. Months with large WAI are featured with amplified waveguide teleconnections along the PFJ, whereas months with near-average WAI are featured with attenuated waveguide teleconnections along the PFJ. The British-Baikal Corridor (BBC) pattern is the dominant wave-like pattern along the PFJ (Xu et al., 2019), but a high WAI does not necessarily mean an active BBC pattern because there may exist other waveguide teleconnections along the PFJ.

3. Results

Figure 2a shows the PDFs of normalized WAI along PFJ in all summer months (black line; 62-year climatology) and in the 30 summer months with the largest |Ts′| anomalies (colored shading) over northern Eurasia. Months with largest |Ts′| anomalies are generally associated with significantly amplified WAI along the PFJ, suggesting that waveguide teleconnections with large amplitude occur relatively more often during months with extreme temperature anomalies than they do climatologically. The statistical significance of the difference in mean WAI between extreme months and climatology is very high ($p < 0.01$). By contrast, months with the smallest |Ts′| anomalies are generally associated with significantly attenuated WAI along the PFJ (Figure 2f), indicating weaker waveguide teleconnections

occur more often during months with near-average temperature anomalies than they do climatologically. The difference in mean WAI between near-average months and climatology is also highly statistically significant ($p < 0.01$).

Analogous PDFs in the 5% summer months with the largest and smallest |Ts'| anomalies are presented from LE simulations using NCAR-CESM1 (Figures 2b and 2g), GFDL-CM3 (Figures 2c and 2h), CCCma-CanESM2 (Figures 2d and 2i), and CSIRO-MK3.6 (Figures 2e and 2j). Here, the calculations are first performed for each member independently and then averaged together for each model. The LE simulations again indicate that extreme months feature amplified WAI, compared to climatology, and near-average months feature attenuated WAI, compared to climatology. The differences in composite-mean WAI compared to climatology are statistically significant for both extreme months and near-normal months in all models. The similarity of the results in observations and model outputs, presented in Figure 2, suggests a robust positive relationship between waveguide teleconnection activities along the PFJ and surface temperature extremes.

So far, we have demonstrated a close relationship between waveguide teleconnections along the PFJ and extreme temperatures for northern Eurasia as a whole. To examine the effects of waveguide teleconnections at the local scale, Figures 3a and 3b present the composite-mean WAI during the 30 summer months with the largest and smallest |Ts'| at every grid point in observations, respectively. Here, the months in each composite are defined based on |Ts'| at each grid point, but the WAI remains the same as in Figure 2 (i.e., area-averaged |V250'| over the Eurasian region). In this way, we can determine how months of extreme or near-normal temperatures at every grid point are related to the amplitude of waveguide teleconnections over northern Eurasia. In other words, interpretations of Figures 3a–3b can show how the amplitude of waveguide teleconnections along the PFJ behaves when a grid point experienced temperature extreme or near-normal temperature. This is similar to Table 1 of Screen and Simmonds (2014), but here we further extend the analysis to each grid point of the northern Eurasia.

Figure 3a shows that at almost all locations, the WAI tends to be amplified during summer months with extreme temperatures. Moreover, the magnitude of this relationship shows a distinct regional variation (Figure 3a). The WAI is most strongly amplified during months of extreme temperatures over central and eastern Europe (~30°E), western Russia (~60°E), and far-eastern Russia (140°E). A broadly similar pattern, but of reversed sign and weaker amplitude, can also be seen for the near-normal conditions (Figure 3b). The geographical variations in the magnitude of the relationship between the extreme temperature and WAI resembles the structure of the BBC pattern (Xu et al., 2019) to some extent. This result indicates the essential role of the BBC pattern in anchoring the surface temperature extremes over the northern Eurasia, though the WAI is defined to measure the overall Rossby wave packets along the PFJ.

Figures 3c–3j present the composite-mean WAI during the 5% summer months with the largest and smallest |Ts'| in LE simulations. The LE simulations further confirm the clear relationship between local temperature extremes and WAI. Although not all the geographical variability of the observed relationship is seen in all the models, there is agreement across all models of especially high and low WAI associated with extreme and near-normal temperatures, respectively, in western Russia (~60°E) compared to other regions (Figures 3c–3j). The WAI anomalies over the eastern and northern Siberia are weaker in some models than observed during the months of extreme temperature and are more spatially homogeneous than observed during the months of near-average temperature. This discrepancy may be due to the systematic biases in the models. However, we note that the discrepancy could also result from the larger sample size of the LE simulations and could indicate that the pattern seen in observation in these regions is not robust.

It is possible that in any particular location, amplified teleconnections may favor one sign of temperature extreme more than another, as suggested in Screen and Simmonds (2014). Figures 4a and 4b present the composite WAI for the 30 summer months with the largest positive and negative Ts' in observations, respectively, for each grid point over northern Eurasia. Here, the figure is constructed in the same manner as Figure 3, but the selected months are based on temperature (i.e., hot/cold) instead of the absolute value of temperature (i.e., extreme/near-normal). Although both hot and cold extremes are linked to amplified WAI in most regions, at a given location, there are stronger links between WAI and temper-

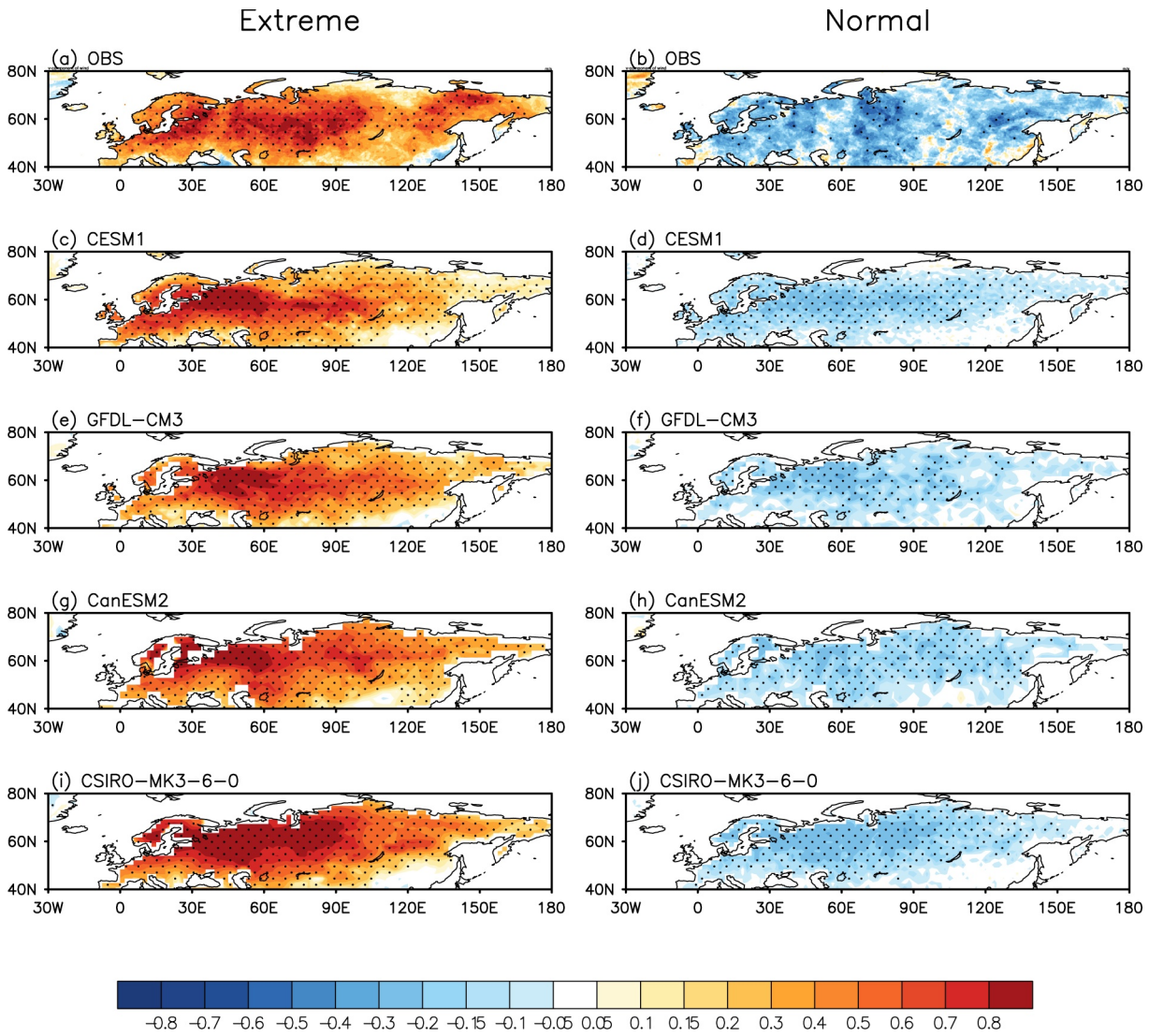

Figure 3. (a) Composite difference of the normalized wave activity index (WAI) between summer months of extreme temperature and climatology. (b) is the same as (a), but during months of near normal temperature. The WAI is defined the same as in Figure 2, that is, the area-averaged |V250'| over Eurasia (15°W–180°E, 50°N–80°N), while the extreme (in a) and near-normal (in b) months are selected based on the |Ts'| at each grid-point. (c) and (d), (e) and (f), (g) and (h), and (i) and (j) are the same as (a) and (b), but for LE simulations of NCAR-CESM1, GFDL-CM3, CCCma-CanESM2, and CSIRO-MK3.6, respectively. Dots indicate the 95% confidence levels based on a two-tailed Student's *t* test.

ature extremes of one sign than the other. For example, amplified waveguide teleconnections are particularly strong during observed hot extremes over eastern Europe and western Russia, and far-eastern Russia (Figure 4a). In contrast, amplified waveguide teleconnections are most obvious during cold extremes over central and eastern Siberia (Figure 4b). Figures 4c–4j present the composite-mean WAI during the 5% summer months with the largest and smallest Ts' in LE simulations. The models reproduce the major spatial features of the observed relationship, for example, the strongly amplified waveguide teleconnections during hot months over eastern Europe and western Russia and the strongly amplified waveguide teleconnections during cold months over central Russia. Again, there are some discrepancies in the models compared to observations. The models generally simulate a more spatially homogeneous feature than observed for both hot extremes (Figures 4c, 4e, 4g, and 4i) and cold extremes (Figures 4d, 4f, 4h, and 4j).

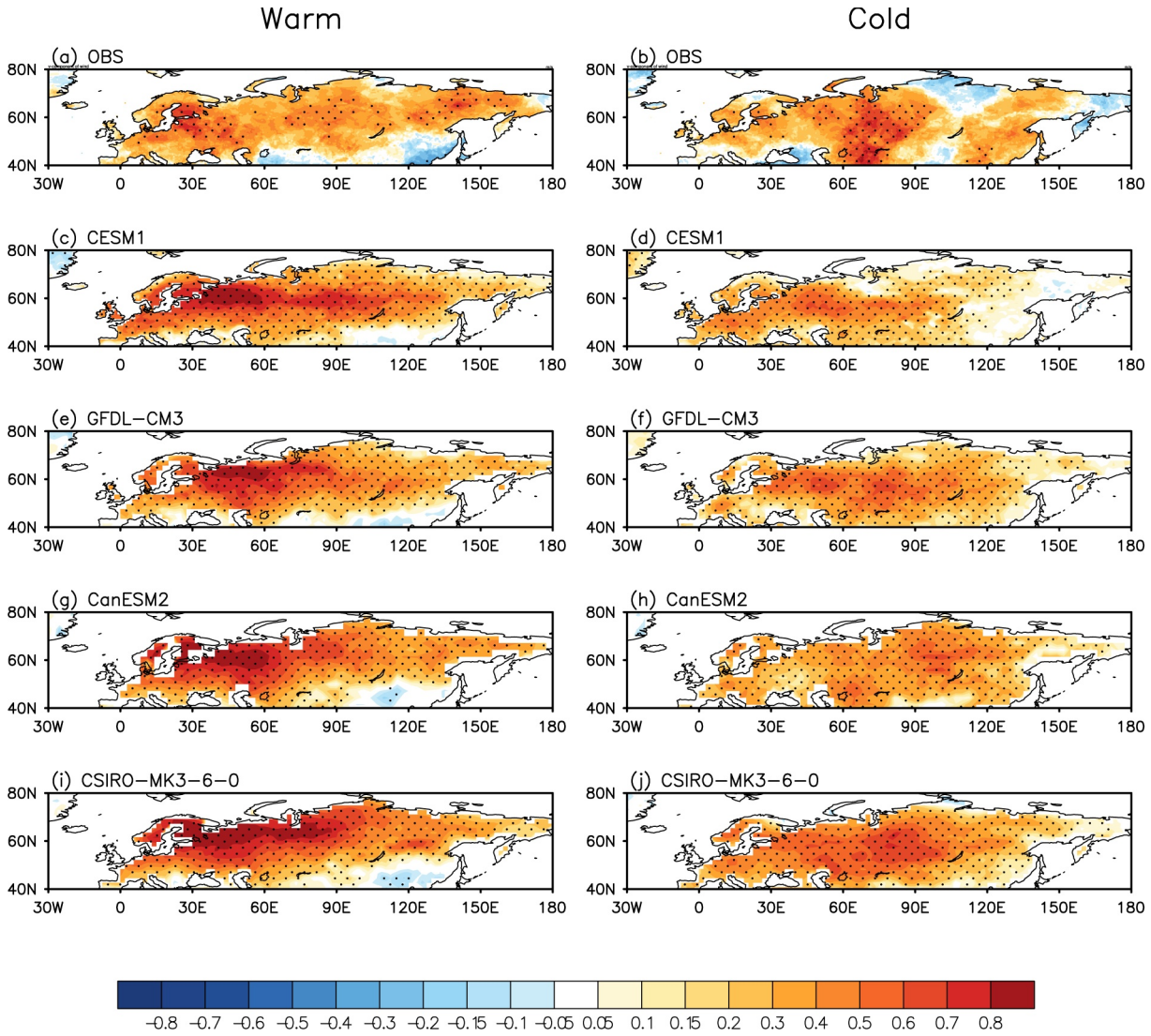

Figure 4. (a) Composite difference of the normalized wave activity index (WAI) between summer months of extremely hot temperature anomalies and climatology for each grid point. (b) is the same as (a), but during summer months of extremely cold temperature anomalies. The WAI is defined the same as in Figure 2, that is, the area-averaged |V250'| over Eurasia (15°W–180°E, 50°N–80°N), while the warm (in a) and cold (in b) months are selected based on the Ts' at each grid-point. (c) and (d), (e) and (f), (g) and (h), and (i) and (j) are the same as (a) and (b), but for LE simulations of NCAR-CESM1, GFDL-CM3, CCCma-CanESM2, and CSIRO-MK3.6, respectively. Dots indicate the 95% confidence levels based on a two-tailed Student's *t* test.

4. Conclusions

It is known that there are close relationships between the waveguide teleconnection activity along the subtropical jet and temperature extremes in the middle latitudes (Screen & Simmonds, 2014). In this paper, we have shown that, in boreal summer, when the waveguide effect of the polar front jet (PFJ) is strong, and the geographical boundary between the PFJ and the subtropical jet is clear, similar relationships also hold for waveguide teleconnections along the PFJ and temperature extremes over northern Eurasia. Those months with extreme temperature anomalies are generally associated with significantly amplified waveguide teleconnections along the PFJ, whereas months with near-average temperature anomalies are generally associated with significantly attenuated waveguide teleconnections along the PFJ. At a local scale, amplified waveguide teleconnections along the PFJ favor high-temperature extremes over eastern Europe, western Russia, and far-eastern Russia and cold temperature extremes over central and eastern Siberia. The results identified in observations are reasonably well reproduced in the LE simulations of four CMIP5-class

models, though the models generally produce weaker signals over eastern and northern Siberia and more spatially homogeneous features compared to observations.

This study demonstrates the robust relationship between the waveguide teleconnections and temperature extremes over northern Eurasia, both in observations and models. Despite this robust result, it remains open whether waveguide teleconnections are the dominant drivers that accumulate the heat to build up and escalate the surface temperature anomalies into extreme values. In the extratropical regions, temperature extremes can be broadly contextualized by considering the larger-scale atmospheric dynamics that favor the thermodynamical processes and land-atmosphere feedbacks (Horton et al., 2016). It means that atmospheric dynamical processes (e.g., atmospheric teleconnections) are intrinsically coupled with both the thermodynamical processes (e.g., clouds and incoming shortwave radiations) and land-atmosphere feedbacks (e.g., soil moisture-temperature coupling process and soil moisture-atmospheric boundary layer coupling process). Nevertheless, the broad similarity between the spatial patterns of surface meridional wind variance associated with amplified waveguide teleconnections and surface temperature variance (Schneider et al., 2015) suggests waveguide teleconnections is a crucial pre-condition for the temperature extremes (figure not shown).

The findings of this study provide a better understanding of the driving mechanisms of summer temperature extremes over northern Eurasia and suggest a potential source of predictability of such events. Given the close relationship between waveguide teleconnections along the PFJ and temperature extremes in the summer, our results motivate further work to assess the impact of global warming and, in particular, polar amplification on the PFJ waveguide and associated waveguide teleconnections.

Conflict of Interest

The authors declare no conflicts of interest relevant to this study.

Data Availability Statement

The JRA55 reanalysis data set is publicly available at https://jra.kishou.go.jp/JRA-55/index_en.html. The CRU data set is publicly available at https://crudata.uea.ac.uk/cru/data/hrg/. The LEs outputs are publicly available from the Earth System Grid (http://www.earthsystemgrid.org).

Acknowledgments
The authors thank the two anonymous reviewers for their insightful comments that led to significant improvement of the paper. P. Xu and L. Wang were supported by the National Natural Science Foundation of China (41925020, 42005057), the China Postdoctoral Science Foundation (2020M670418), and the Special Research Assistant Project of the Chinese Academy of Sciences. G. K. Vallis, R. Geen, and P. Wu were supported by the UK-China Research and Innovation Partnership Fund, through the Met Office Climate Science for Service Partnership (CSSP) China, as part of the Newton Fund. J. A. Screen was supported by the NERC grant NE/P006760/1. Part of the work was performed when P. Xu visited the University of Exeter under the support of the CSSP-China project.

References

Alexander, L., & Perkins, S. (2013). Debate heating up over changes in climate variability. *Environmental Research Letters*, *8*(4), 041001. https://doi.org/10.1088/1748-9326/8/4/041001

Barriopedro, D., Fischer, E. M., Luterbacher, J., Trigo, R. M., & García-Herrera, R. (2011). The hot summer of 2010: Redrawing the temperature record map of Europe. *Science*, *332*(6026), 220–224. https://doi.org/10.1126/science.1201224

Blackport, R., & Screen, J. A. (2020a). Insignificant effect of Arctic amplification on the amplitude of midlatitude atmospheric waves. *Science Advances*, *6*(8), eaay2880. https://doi.org/10.1126/sciadv.aay2880

Blackport, R., & Screen, J. A. (2020b). Weakened evidence for mid-latitude impacts of Arctic warming. *Nature Climate Change*, *10*(12), 1065–1066. https://doi.org/10.1038/s41558-020-00954-y

Branstator, G. (2002). Circumglobal teleconnections, the jet stream waveguide, and the North Atlantic Oscillation. *Journal of Climate*, *15*(14), 1893–1910. https://doi.org/10.1175/1520-0442(2002)015<1893:cttjsw>2.0.co;2

Branstator, G., & Teng, H. (2017). Tropospheric waveguide teleconnections and their seasonality. *Journal of the Atmospheric Sciences*, *74*(5), 1513–1532. https://doi.org/10.1175/jas-d-16-0305.1

Chowdary, J. S., Hu, K., Srinivas, G., Kosaka, Y., Wang, L., & Rao, K. K. (2019). The Eurasian jet streams as conduits for East Asian monsoon variability. *Current Climate Change Reports*, *5*(3), 233–244. https://doi.org/10.1007/s40641-019-00134-x

Coumou, D., Di Capua, G., Vavrus, S., Wang, L., & Wang, S. (2018). The influence of Arctic amplification on mid-latitude summer circulation. *Nature Communications*, *9*(1), 1–12. https://doi.org/10.1038/s41467-018-05256-8

Coumou, D., & Robinson, A. (2013). Historic and future increase in the global land area affected by monthly heat extremes. *Environmental Research Letters*, *8*(3), 034018. https://doi.org/10.1088/1748-9326/8/3/034018

Coumou, D., Robinson, A., & Rahmstorf, S. (2013). Global increase in record-breaking monthly-mean temperatures. *Climatic Change*, *118*(3), 771–782. https://doi.org/10.1007/s10584-012-0668-1

Deser, C., Lehner, F., Rodgers, K. B., Ault, T., Delworth, T. L., DiNezio, P. N., et al. (2020). Insights from Earth system model initial-condition large ensembles and future prospects. *Nature Climate Change*, *10*(4), 277–286. https://doi.org/10.1038/s41558-020-0731-2

Ding, Q. H., & Wang, B. (2005). Circumglobal teleconnection in the Northern Hemisphere summer. *Journal of Climate*, *18*(17), 3483–3505. https://doi.org/10.1175/jcli3473.1

Francis, J. A., & Vavrus, S. J. (2012). Evidence linking Arctic amplification to extreme weather in mid-latitudes. *Geophysical Research Letters*, *39*(6), L06801. https://doi.org/10.1029/2012gl051000

Harris, I., Osborn, T. J., Jones, P., & Lister, D. (2020). Version 4 of the CRU TS monthly high-resolution gridded multivariate climate dataset. *Scientific Data*, *7*(1), 109. https://doi.org/10.1038/s41597-020-0453-3

Horton, R. M., Mankin, J. S., Lesk, C., Coffel, E., & Raymond, C. (2016). A review of recent advances in research on extreme heat events. *Current Climate Change Reports*, *2*, 242–259. https://doi.org/10.1007/s40641-016-0042-x

Iwao, K., & Takahashi, M. (2008). A precipitation seesaw mode between Northeast Asia and Siberia in summer caused by Rossby waves over the Eurasian continent. *Journal of Climate*, *21*(11), 2401–2419. https://doi.org/10.1175/2007jcli1949.1

Jeffrey, S., Rotstayn, L., Collier, M., Dravitzki, S., Hamalainen, C., Moeseneder, C., et al. (2013). Australia's CMIP5 submission using the CSIRO-Mk3.6 model. *Australian Meteorological and Oceanographic Journal*, *63*(1), 1–14. https://doi.org/10.22499/2.6301.001

Kay, J. E., Deser, C., Phillips, A., Mai, A., Hannay, C., Strand, G., et al. (2015). The Community Earth System Model (CESM) large ensemble project: A community resource for studying climate change in the presence of internal climate variability. *Bulletin of the American Meteorological Society*, *96*(8), 1333–1349. https://doi.org/10.1175/bams-d-13-00255.1

Kirchmeier-Young, M. C., Zwiers, F. W., & Gillett, N. P. (2017). Attribution of extreme events in Arctic sea ice extent. *Journal of Climate*, *30*(2), 553–571. https://doi.org/10.1175/jcli-d-16-0412.1

Kobayashi, S., Ota, Y., Harada, Y., Ebita, A., Moriya, M., Onoda, H., et al. (2015). The JRA-55 reanalysis: General specifications and basic characteristics. *Journal of the Meteorological Society of Japan*, *93*(1), 5–48. https://doi.org/10.2151/jmsj.2015-001

Liu, J., Curry, J. A., Wang, H., Song, M., & Horton, R. M. (2012). Impact of declining Arctic sea ice on winter snowfall. *Proceedings of the National Academy of Sciences*, *109*(11), 4074–4079. https://doi.org/10.1073/pnas.1114910109

Mann, M. E., Rahmstorf, S., Kornhuber, K., Steinman, B. A., Miller, S. K., & Coumou, D. (2017). Influence of anthropogenic climate change on planetary wave resonance and extreme weather events. *Scientific Reports*, *7*, 45242. https://doi.org/10.1038/srep45242

Nakamura, H., & Fukamachi, T. (2004). Evolution and dynamics of summertime blocking over the Far East and the associated surface Okhotsk high. *Quarterly Journal of the Royal Meteorological Society*, *130*(599), 1213–1233. https://doi.org/10.1256/qj.03.101

Petoukhov, V., Rahmstorf, S., Petri, S., & Schellnhuber, H. J. (2013). Quasiresonant amplification of planetary waves and recent Northern Hemisphere weather extremes. *Proceedings of the National Academy of Sciences of the United States of America*, *110*(14), 5336–5341. https://doi.org/10.1073/pnas.1222000110

Schneider, T., Bischoff, T., & Plotka, H. (2015). Physics of changes in synoptic midlatitude temperature variability. *Journal of Climate*, *28*(6), 2312–2331. https://doi.org/10.1175/jcli-d-14-00632.1

Schubert, S., Wang, H., & Suarez, M. (2011). Warm season subseasonal variability and climate extremes in the Northern Hemisphere: The role of stationary Rossby waves. *Journal of Climate*, *24*(18), 4773–4792. https://doi.org/10.1175/jcli-d-10-05035.1

Screen, J. A., & Simmonds, I. (2013). Caution needed when linking weather extremes to amplified planetary waves. *Proceedings of the National Academy of Sciences*, *110*(26), E2327. https://doi.org/10.1073/pnas.1304867110

Screen, J. A., & Simmonds, I. (2014). Amplified mid-latitude planetary waves favor particular regional weather extremes. *Nature Climate Change*, *4*(8), 704–709. https://doi.org/10.1038/nclimate2271

Sousa, P. M., Barriopedro, D., García-Herrera, R., Ordóñez, C., Soares, P. M. M., & Trigo, R. M. (2020). Distinct influences of large-scale circulation and regional feedbacks in two exceptional 2019 European heatwaves. *Communications Earth & Environment*, *1*(1), 48. https://doi.org/10.1038/s43247-020-00048-9

Sun, L., Alexander, M., & Deser, C. (2018). Evolution of the global coupled climate response to Arctic sea ice loss during 1990–2090 and its contribution to climate change. *Journal of Climate*, *31*(19), 7823–7843. https://doi.org/10.1175/jcli-d-18-0134.1

Tang, Q., Zhang, X., & Francis, J. A. (2014). Extreme summer weather in Northern mid-latitudes linked to a vanishing cryosphere. *Nature Climate Change*, *4*(1), 45–50. https://doi.org/10.1038/nclimate2065

Teng, H., & Branstator, G. (2019). Amplification of waveguide teleconnections in the boreal summer. *Current Climate Change Reports*, *5*(4), 421–432. https://doi.org/10.1007/s40641-019-00150-x

Teng, H., Branstator, G., Meehl, G. A., & Washington, W. M. (2016). Projected intensification of subseasonal temperature variability and heat waves in the Great Plains. *Geophysical Research Letters*, *43*(5), 2165–2173. https://doi.org/10.1002/2015gl067574

Trenberth, K. E., & Fasullo, J. T. (2012). Climate extremes and climate change: The Russian heat wave and other climate extremes of 2010. *Journal of Geophysical Research*, *117*(D17). https://doi.org/10.1029/2012jd018020

Wills, R. C. J., White, R. H., & Levine, X. J. (2019). Northern hemisphere stationary waves in a changing climate. *Current Climate Change Reports*, *5*(4), 372–389. https://doi.org/10.1007/s40641-019-00147-6

Xu, P., Wang, L., & Chen, W. (2019). The British-Baikal Corridor: A teleconnection pattern along the summertime polar front jet over Eurasia. *Journal of Climate*, *32*(3), 877–896. https://doi.org/10.1175/jcli-d-18-0343.1

Xu, P., Wang, L., Chen, W., Chen, G., & Kang, I.-S. (2020). Intraseasonal variations of the British-Baikal Corridor pattern. *Journal of Climate*, *33*(6), 2183–2200. https://doi.org/10.1175/jcli-d-19-0458.1

Xu, P., Wang, L., Huang, P., & Chen, W. (2021). Disentangling dynamical and thermodynamical contributions to the record-breaking heatwave over Central Europe in June 2019. *Atmospheric Research*, *252*, 105446. https://doi.org/10.1016/j.atmosres.2020.105446

Xu, P., Wang, L., Liu, Y., Chen, W., & Huang, P. (2020). The record-breaking heat wave of June 2019 in Central Europe. *Atmospheric Science Letters*, *21*(4), e964. https://doi.org/10.1002/asl.964